Measurement 206 (2023) 112216

Contents lists available at ScienceDirect

Measurement

journal homepage: www.elsevier.com/locate/measurement

Vehicle assisted bridge damage assessment using probabilistic deep learning

Muhammad Zohaib Sarwar *, Daniel Cantero

Department of Structural Engineering, Norwegian University of Science & Technology, Trondheim, Norway

ARTICLE INFO

Keywords:
Vehicle assisted monitoring
Damage assessment
Highway bridges
Probabilistic deep learning
Fully connected neural network
Uncertainty quantification

ABSTRACT

Vehicle assisted monitoring has shown promising potential for the condition assessment of existing bridges in a road network, by removing practical complications faced in traditional Structural health monitoring (SHM) methods such as traffic interruption and dense deployment of sensors. However, the combination of different measurement sources during vehicle assisted monitoring has not yet been fully explored. This paper aims to evaluate the potential benefit of considering multiple measured responses from various sources, including fixed sensors on the bridge and on-board vehicle sensors. To this end, this paper proposes a Probabilistic Deep Neural Network, a stochastic data-driven framework for damage assessment. This framework enables the combination of vehicle and bridge responses to extract damage sensitive features for the classification of different damage states. In addition, the proposed method estimates the uncertainty of its predictions, providing an indication of the reliability of the result. The proposed method is validated using two numerical based case studies while considering realistic operational conditions, which include temperature oscillations, additional traffic, and measurement noise. The results from this study indicate that combining multiple sensor information results in lower uncertainties in damage detection and localisation. The results also suggest that the proposed method is robust in handling measurement noise and varying environmental conditions.

1. Introduction

The growing stock of bridges is continuously subjected to deterioration caused by different factors, such as excessive loading, fatigue, corrosion, and environmental impact [1]. A failure to identify these damages at an early stage can lead to catastrophic outcomes in terms of human life and the economy. Currently, for safe and reliable operation of bridges, visual inspection based methods are in practice, which are generally expensive and prone to errors [2]. With recent advancements in sensing technologies and data acquisition systems, vibration-based health monitoring solutions are promising alternatives for effective and accurate tracking of the structural deterioration processes [3]. These methods mainly rely on the detection of damage and potential anomalies by analysing the dynamic response of bridges.

Vibration-based Structural Health Monitoring (SHM) systems can be categorised into fixed or mobile sensing frameworks. In a fixed sensing framework, the sensors are directly installed at a fixed location of the target bridge. There are three main challenges associated to this framework. First, the extensive deployment requirements in terms of cost and labour, that is generally prohibitive for the inspection of short to medium span bridges. Second, the spatial information obtained with a fixed sensing system is mainly confined to certain discrete locations, which adversely affects the outcome of the bridge's assessment. The third main challenge is that often the collected vibration data is obtained during ambient and forced vibration. However, the bridge response induced by ambient vibrations and random traffic loading may not be sufficiently big to excite the stiff bridge properly and the measured responses are often corrupted by measurement noise [4]. While forced vibration responses can be obtained using impact load testing, human-induced loads or by applying hydraulic actuators, which in practice significantly affect the serviceability of the bridge and increase maintenance costs. In recent years Vehicle assisted monitoring is an active research topic. In vehicle assisted monitoring, traversing vehicles are used as the source of excitation. The forced response of the bridge is measured using installed sensors on the bridge or sensors installed inside the moving vehicles. With this framework the process of the bridge's excitation becomes relevantly economical and bridge vibration data is only acquired when the vehicle is on the bridge. Moreover, when vehicles are acting as mobile sensors, the measured responses contain all the spatial information of the target bridge, which significantly improves the condition assessment of bridges [5].

In recent years, many researchers have explored vehicle assisted monitoring systems to perform damage assessment. Shokravi et al. [6] conducted a comprehensive review on conventional vehicle assisted bridge damage assessment techniques. These techniques can be categorised into direct (fixed sensing) or indirect (mobile sensing). Using direct sensing, [5,7] applied Moving Force Identification (MFI)

* Corresponding author.
E-mail addresses: muhammad.z.sarwar@ntnu.no (M.Z. Sarwar), daniel.cantero@ntnu.no (D. Cantero).

https://doi.org/10.1016/j.measurement.2022.112216
Received 19 August 2022; Received in revised form 3 November 2022; Accepted 14 November 2022
Available online 21 November 2022

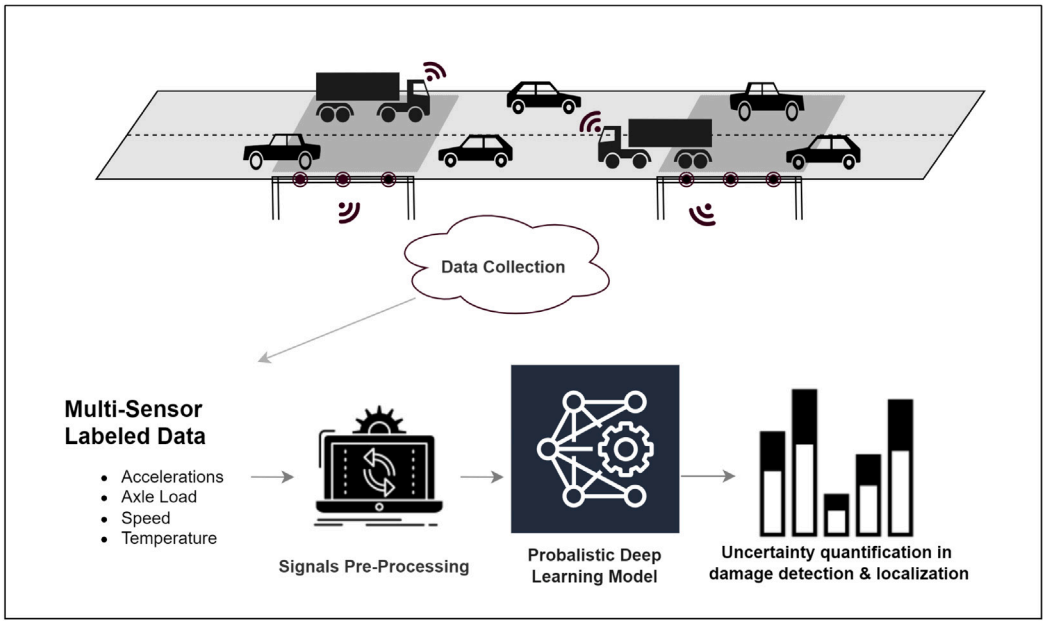

Fig. 1. Main overview of proposed framework.

method for bridge damage assessment. Furthermore, in [8,9] the authors utilised the measured rotational response of a bridge under the influence of moving loads for damage assessment. On the other hand, indirect techniques (or drive-by) have also been studied for bridge damage assessment, of which Wang et al. [10] provide a detailed overview of their application. The reported methods mainly rely on advanced signal processing techniques and machine learning methods for damage detection. For instance, [11,12] used data driven techniques and statistical analysis for damage detection and quantification. While [13,14] estimate the contact point response between vehicle and bridge for damage detection and localisation.

Therefore, it can be concluded that vehicle assisted monitoring systems have great potential to be used for damage assessment. The reported methods have limitations and face unaddressed challenges, which include the influence of vehicle speed, the effect of road profile and additional random traffic, and the requirement of specialised vehicles, among others. However, considering the merits of direct and indirect methods, it is possible that the combination of both strategies could be advantageous and complement each other. The combination of recent advancements in wireless sensing systems to instrument the infrastructure together with the increasing trend of equipping vehicles with multiple sensors, opens the possibility for Vehicle to Infrastructure (V2I) connectivity. This integration has shown potential benefits to improve traffic and resources management [15,16]. However, to the author's best knowledge this interconnectivity between vehicle and bridge sensors has not been fully explored in the context of damage assessment and bridge maintenance.

Traditionally, free and ambient vibration responses have been used for SHM relying on the assumption that the acquired structural responses are linear and stationary. However, this assumption does not hold when the bridge is exited by a moving vehicle, when the structural dynamic properties are time-varying making the response nonstationary. Then, combining multi-variant data (fixed sensors and moving sensors) and extracting damage sensitive features is a challenging task. Recently, Deep Learning (DL) models are getting significant attention in SHM applications. Deep learning models are tools that can be used to find complex non-linear correlations within the datasets. These models have the ability to combine multi-sensor data and perform various tasks, including non-linear feature extraction, classification and regression. For damage assessment, Ni et al. [17] and Zhang et al. [18] used a 1-D Convolutional Neural Network (CNN) to extract damage sensitive features from acceleration responses. Zhang et al. [19] used phase motion estimation and CNN for damage detection application. In [20,21] applied the CNN based method for condition assessment of engine valve and rolling bearings. Similarly, for bridge health monitoring Ma et al. [22] applied a convolutional variational autoencoder to compress the high-dimensional data to a low-dimensional feature space, which was then used to establish a damage index, and validated experimentally. In [23], the authors proposed the idea of the natural excitation technique for data normalisation and then applied 1-D CNN for automated damage detection. Nevertheless, the practical implementation of DL models for SHM is hindered because the collected training data does not contain all operational and loading conditions, which would facilitate the quantification of the uncertainty in decision output of the model. For reliable decision making, the SHM system must be able to handle uncertainty in its predictions.

Therefore, the goal of this study is to develop a damage assessment method for bridges by combining forced response data obtained from fixed and moving sensors, capable of quantifying the uncertainties of the output. This study presents a data-driven method for damage assessment using vehicle assisted monitoring data. The main overview of the proposed framework is shown in Fig. 1, where data from multiple sources is collected. The gathered data is further analysed using advanced data-driven methods for damage assessment. A probabilistic Deep Neural Network (PDNN) based framework is developed in order to extract damage sensitive features and account for uncertainty in predictions. The framework leverages the usage of probabilistic neural layers, which can represent the problem's uncertainties. Monte Carlo analysis is used to sample the weights from trained models to predict different damage states. To evaluate the performance of the proposed approach, ten different information scenarios (signal source combinations) are considered for training each PDNN. The idea is validated numerically for two types of bridges traversed by 5-axle trucks. The study considers a range of vehicle dynamic properties and the presence of road profile and evaluates the effect ambient temperature variations, additional traffic, and measurement noise.

The remainder of the paper is organised as follows. Section 2 provides an overview of the proposed deep learning strategy, including architecture of the model and implementation details. Section 3 presents the details of the vehicle-bridge interaction model used to generate the datasets. Section 4 evaluates the performance of the proposed

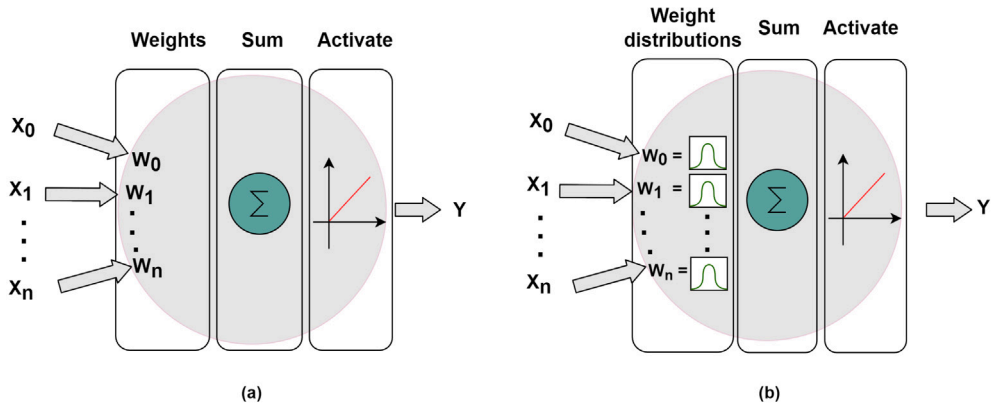

Fig. 2. Basic ANN model; (a) with deterministic weights; (b) with probabilistic weights.

method for two case studies, a simply supported bridge and a multi-span continuous bride. Section 5 provide the discussion on overall finding of the proposed studies. Section 6 summarises the findings of this study.

2. Deep learning model

2.1. Research significance

Deep Learning (DL) based models are widely used in SHM applications, including damage assessment. In that case, these models provide solutions to tackle the problem of differentiating among large number of damage classes [1]. However, DL models are prone to underfitting or overfitting, which affect their generalisation capabilities for the given data [24]. What is more, these models also tend to be overconfident in their predictions and do not account for the inherent uncertainties [25] of the problem. To overcome these issues, probabilistic deep learning based models have been proposed. These models provide the framework to account for the uncertainty in their predictions. Probabilistic Deep Neural Networks (PDNN) are stochastic artificial neural networks that are trained by using a Bayesian approach [26].

2.2. Probabilistic deep neural network

Standard Deep Neural Network (DNN) are built using an input layer $\boldsymbol{l_0}$, multiple hidden layers $\boldsymbol{l}_i$ (for $i = 1, 2, \ldots, n-1$) with non-linear operations, and a final output layer $\boldsymbol{l}_o$. For a simple feedforward network, each layer $\boldsymbol{l}$ is composed of linear transformation and activation function denoted as α. The goal in a simple DNN is to approximate an arbitrary function $\boldsymbol{Y} = \boldsymbol{\Phi}(\boldsymbol{X})$, based on the input $\boldsymbol{X}$. Their architecture can be summarised as follows:

$$\begin{aligned} &\boldsymbol{l_0} = \boldsymbol{X}, \\ &\boldsymbol{l}_i = \alpha(\boldsymbol{W}_i \boldsymbol{l}_{i-1} + \boldsymbol{b}_i) \quad i \in [1, n], \\ &\boldsymbol{Y} = \boldsymbol{l}_n \end{aligned} \tag{1}$$

Here, n is the number of hidden layers while $\boldsymbol{W}$ and $\boldsymbol{b}$ are the weights and biases of the network. These learning parameters $\boldsymbol{\theta} = (\boldsymbol{W}, \boldsymbol{b})$ are optimised as single deterministic estimates for a given data set (Fig. 2a) using backpropagation algorithm.

On the other hand, stochastic neural networks or PDNN are built by introducing stochastic components into the network [27]. The stochastic neural networks are mainly built to account for two types of uncertainties: either the randomness in the input data or the uncertainties in the estimated parameters of the deep learning model. The first one can be handled by using probability distributions in the loss function as discussed in thoroughly in [28]. While the latter can be accounted for by considering weights as stochastic (Fig. 2b) to simulate multiple possible model parameters $\boldsymbol{\theta}$ with their associated probability distribution $p(\boldsymbol{\theta})$. For this study the main goal of PDNN is to capture the associated uncertainty of the underlying processes. This can be achieved by evaluating predictions of multiple parameterised $\boldsymbol{\theta}$ sampled models. If the outputs of multiple models agree, then the uncertainty is considered to be low. While in the case of extended disagreement in predictions, then the uncertainty is considered as high. The process at a high level can be expressed as:

$$\begin{aligned} &\boldsymbol{\theta} \sim p(\boldsymbol{\theta}), \\ &\boldsymbol{Y} = PDNN_{\theta}(\boldsymbol{X}) + \varepsilon \end{aligned} \tag{2}$$

where ε represents a noise to account for the fact that $PDNN_{\theta}$ is only a probabilistic approximation of a function.

In order to design the PDNN, the first step is to select the architecture of the neural network, namely a fully connected network or a convolutional neural network. Then the second step is to include the selection of prior distributions over the possible model parameters $p(\boldsymbol{\theta})$ and their prior confidence over the predictive power of the model $p(\boldsymbol{Y}|\boldsymbol{X}, \boldsymbol{\theta})$. For supervised learning, Bayesian posteriors can be computed as shown in Eq. (3) by applying Bayes's theorem and considering independence between the input data D and the model parameters $\boldsymbol{\theta}$.

$$p(\boldsymbol{\theta}|D) = \frac{p(D_y|D_x, \boldsymbol{\theta})\, p(\boldsymbol{\theta})}{\int p(D_y|D_x, \boldsymbol{\theta}^*)\, p(\boldsymbol{\theta}^*)\, d\boldsymbol{\theta}^*} \tag{3}$$

where D_x and D_y are training inputs and training labels for the dataset D. In complex models such as deep neural networks, Bayesian posteriors become high dimensional probability distributions. This issue makes computing and sampling using the standard method an intractable problem, especially computing the evidence (denominator) in Eq. (3). To mitigate this problem and for practical implementation, variational inference is applied, which learns a variational distribution to approximate the exact posterior. The main idea behind variational inference is to have a prior variational distribution $q_{\phi}(H)$ parameterised by a set of parameters ϕ and then learn those parameters such that it is close to the exact posterior. More details about variational inference can be found in [25]. Therefore, the probabilistic prediction with known posterior can be expressed as:

$$p(\boldsymbol{Y}|\boldsymbol{X}, D) = \int p(Y|X, \boldsymbol{\theta}^*)\, p(\boldsymbol{\theta}^*|\boldsymbol{D})\, d\boldsymbol{\theta}^* \tag{4}$$

Eq. (4) can be interpreted as the predictive distribution of an infinite ensemble of networks. In practice $p(\boldsymbol{Y}|\boldsymbol{X}, D)$ is sampled indirectly from Eq. (2). The final prediction can be computed via a Monte Carlo analysis [29] by using a finite number of randomly sampled weight parameters from the posterior to compute the series of possible outputs as shown in Fig. 3. In order to measure the uncertainty in the classification problem the average model prediction will give the probability of each class, which can be computed as follows:

$$\hat{\boldsymbol{p}} = \frac{1}{N} \sum_{\theta_i \in \boldsymbol{N}} PDNN_{\theta_i}(\boldsymbol{X}) \tag{5}$$

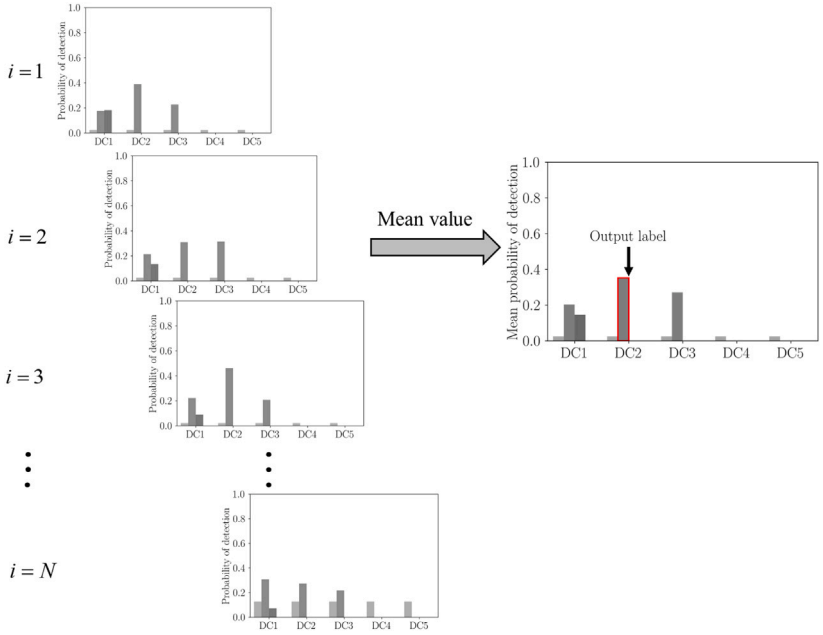

Fig. 3. Illustration to compute final prediction for single input using probabilistic deep neural network.

where N is the number of total samples used for the Monte Carlo analysis. To get the final prediction as shown in Fig. 3, the most likely class can be taken as:

$$\hat{\boldsymbol{Y}} = \arg\max_i p_i \in \hat{\boldsymbol{p}} \tag{6}$$

2.3. Network architecture of probabilistic deep neural network

In recent years, Fully Convolutional Neural networks (FCN) have shown the state of the art performance in classifying time series datasets for a wide range of fields, including SHM [1,30]. FCN has been mainly developed to avoid the demanding pre-processing and feature extraction task on raw data in classification problems. However, they are mainly limited to univariate time series [31]. Karim et al. [32] proposed the augmentation of FCN with Long Short-Term Memory (LSTM) recurrent neural network. This significantly enhances the performance of FCN with a nominal increase in computational cost and has also shown satisfactory performance on various multivariate time series datasets [33]. The network architecture proposed in this paper is mainly inspired by [33] with some modifications according to the problem at hand.

For vehicle assisted damage assessment, the input dataset would include information from multiple sensors (vehicle speed, axle loads, acceleration responses and temperature). The proposed neural network is designed to utilise all (or parts) of this information. The proposed model is mainly divided into two modules, as shown in Fig. 4. The first module takes the time series measurements as input. The architecture of this module is similar to what is proposed in [33]. This module includes three temporal convolutional blocks used as a feature extractor. Each convolutional block includes convolutional layers with filter sizes 128, 256 and 128, strides value as 2 and a kernel size of 7, 5 and 3 respectively. Each convolutional layer is followed by a non-linear activation function (ReLU). In addition to that, it is assumed that the bias and kernel in the convolutional layers are drawn from distributions. Finally, the extracted features are fed into global average pooling layers, which substantially reduces the number of weights of the model, as opposed to feeding the dataset directly to a fully connected layer.

In parallel, the time series input is passed through the dimension shuffle layer. The transformed input is then passed to the LSTM block followed by the activation function and dropout layer. The main goal of this block is to learn the global temporal information of each variable at each time step. The multivariate time series has T time steps (length of signal) and K variables (number of different sensors). Each variable K is defined as a channel of the FCN block. However, if the same data is passed through the LSTM block, then the LSTM would require T time steps to process K variables per time step, which significantly increases the computational cost and adversely affects the efficiency of the model. Instead, the dimension shuffle layer is applied, which effectively transposes the temporal dimension of the input data. After this operation, the input of LSTM now receives the entire time history T of each variable K at each time step. As a result, the LSTM block has global temporal information of each variable at the same time, which significantly helps in improving the overall performance of the model and also reduces the time of training.

In addition, the input data can also have some discrete valued information. In the case of vehicle assisted monitoring, vehicle speed, axle weights and temperature information can be combined to see the overall effect of these features in damage assessment. In order to add these features, the second module is designed using 4 fully connected layers, with layer sizes (32, 64, 64 and 32), followed by the ReLU activation function. Here it is assumed that the bias and kernel in the fully connected layers are also drawn from distributions, as done in the convolutional layers. The output of the last fully connected layer, the global average pooling layer of FCN, and the LSTM block are concatenated and fed into a fully connected layer with Softmax as an activation function for the classification task.

2.4. Implementation

The proposed model is implemented using TensorFlow's probability module and Keras [34]. The FCN convolutional layers are implemented using the convolutional1DFlipout, while DenseFlipout layer is used for the fully connected layers. These layers implement the Bayesian inference by assuming that the bias and kernel are drawn from distributions, which are approximated with the Flipout Monte Carlo estimator [35]. The implementation of each layer assumes the prior for weight $\boldsymbol{W}$ as Gaussian distribution with zero mean μ and unit variance σ^2. For the approximation of the posterior distribution and the classification task,

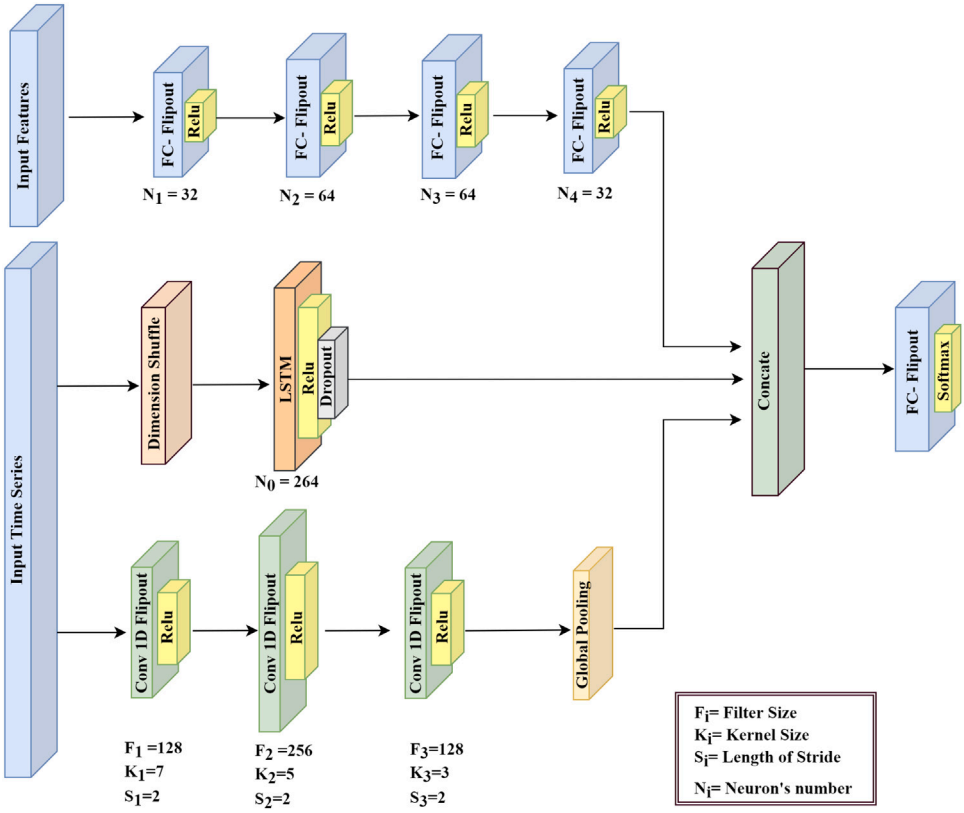

Fig. 4. Architecture of probabilistic deep neural network (PDNN).

Flipout gradient estimator is used to minimise the loss function, called as negative Evidence Lower Bound (ELBO) which is expressed as:

$$\boldsymbol{L}(\boldsymbol{W}_{(\mu,\sigma^2)}) = \arg\min_{\mu,\sigma^2} \sum_{(\boldsymbol{X},\boldsymbol{Y})\in \boldsymbol{D}} log[p(D_y|D_x,\boldsymbol{\theta})] + D_{\mathrm{KL}}(q_\phi \,||\, P) \tag{7}$$

The loss term shown in Eq. (7) is the sum of the negative log-likelihood and the approximated Kullback–Leibler (KL) divergence, which measures the distance between variational and posterior distributions. The KL term here acts as a regularisation term to prevent overfitting on the training dataset.

3. Numerical modelling

This section presents the vehicle-bridge interaction model used to simulate the vehicle responses while traversing a bridge. Fig. 5 shows the schematic representation of the vehicle-bridge coupled system. This numerical model can simulate multiple vehicle crossing events at different speeds, while including the effect of road irregularities. The generated vehicle responses constitute the signals used to evaluate the performance of the proposed PDNN model for damage detection and quantification.

The vehicle model used in this study represents an articulated 5-axle truck with a tractor-trailer configuration. The tractor has two axles and the trailer has three axles at the back. The main bodies of tractor and trailer are modelled as rigid bodies, while the axles are represented as lumped masses. The main bodies are connected to the axle masses by spring and dashpot systems, while the axle masses are connected to the road profile using single springs representing the tyres. The vehicle model has a total of 8 independent Degrees Of Freedom (DOFs) and 1 dependent DOF because of the articulation between tractor and trailer [36,37]. The generic equation of motion of such a vehicle model can be represented as:

$$\boldsymbol{M}_{\boldsymbol{v}}\ddot{u}_v + \boldsymbol{C}_{\boldsymbol{v}}\dot{u}_v + \boldsymbol{K}_{\boldsymbol{v}}u_v = \boldsymbol{F}_{\boldsymbol{v}} \tag{8}$$

In Eq. (8), $\boldsymbol{M}_{\boldsymbol{v}}$, $\boldsymbol{C}_{\boldsymbol{v}}$, and $\boldsymbol{K}_{\boldsymbol{v}}$ are the mass, damping and stiffness matrices, while u_v contains the displacements of all DOFs of the vehicle model. The vehicle parameters and their variability are taken from [12], for the realisation of Monte Carlo simulations. The values of the vehicle parameters are mainly based on European 5-axles trucks and adopted from [38,39]. This study utilises the 5-axle truck model because it is arguably the most frequent heavy vehicle found on European roads.

The bridge is simulated using a Finite Element Model (FEM) representation, consisting of beam elements with 2 nodes and 2 DOFs per node. The bridge has length L, second moment of area I, mass per unit length ρ, and modulus of elasticity E. Eq. (9) represents the equation of motion of the bridge model:

$$\boldsymbol{M}_{\boldsymbol{b}}\ddot{u}_{br} + \boldsymbol{C}_{\boldsymbol{b}}\dot{u}_{br} + \boldsymbol{K}_{\boldsymbol{b}}u_{br} = \boldsymbol{F}_{\boldsymbol{br}} \tag{9}$$

where $\boldsymbol{M}_{\boldsymbol{b}}$, $\boldsymbol{C}_{\boldsymbol{b}}$, and $\boldsymbol{K}_{\boldsymbol{b}}$ are the mass, damping and stiffness matrices, while $\ddot{u}_{br}$, $\dot{u}_{br}$ and u_{br} are the vectors of accelerations, velocities and displacements for each node. To consider the effect of pavement irregularities on the vehicle and bridge responses, the road profile is represented as ISO class A [40]. Fig. 6 shows the road profile generated for the two bridges studied in Section 4. In each figure, the black lines indicate the span of the bridges. In addition, the road profiles have a 100 m approach distance to allow the traversing vehicle to achieve dynamic equilibrium before entering the bridge. In order to represent the contact surface of the truck tyres, a moving average filter of 0.24 m is applied to the profile as suggested in [41].

Finally, to simulate the vehicle-bridge interaction, the equations of motion of the vehicle and bridge models are coupled together into the system of second order differential equations shown in Eq. (10).

$$\boldsymbol{M}_{\boldsymbol{c}}\ddot{u}_c + \boldsymbol{C}_{\boldsymbol{c}}\dot{u}_c + \boldsymbol{K}_{\boldsymbol{v}}u_v = \boldsymbol{F} \tag{10}$$

where in $\boldsymbol{M}_{\boldsymbol{c}}$, $\boldsymbol{C}_{\boldsymbol{c}}$, and $\boldsymbol{K}_{\boldsymbol{c}}$ are the time varying mass, damping and stiffness matrices respectively. The vectors $\ddot{u}_c$, $\dot{u}_c$, and u_c contain the

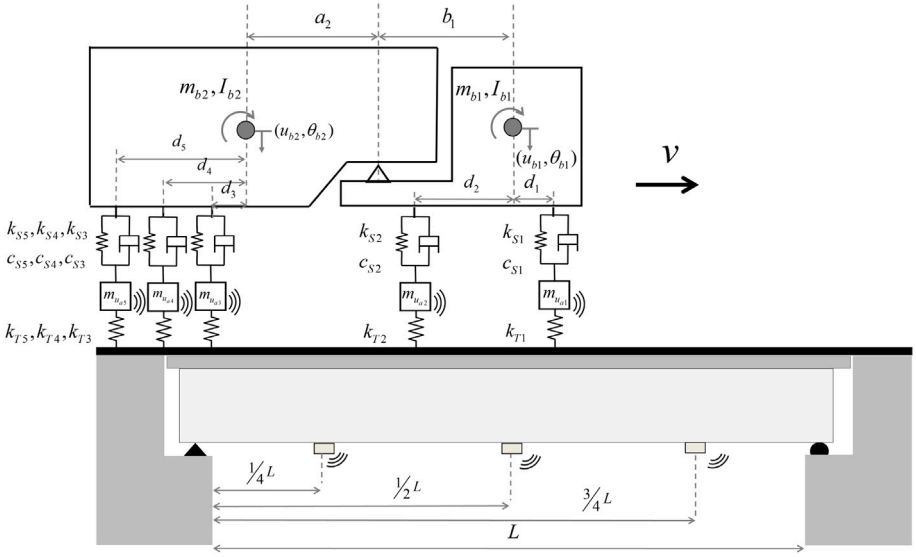

Fig. 5. Vehicle-bridge interaction model for a 5-axle truck traversing a simply supported bridge.

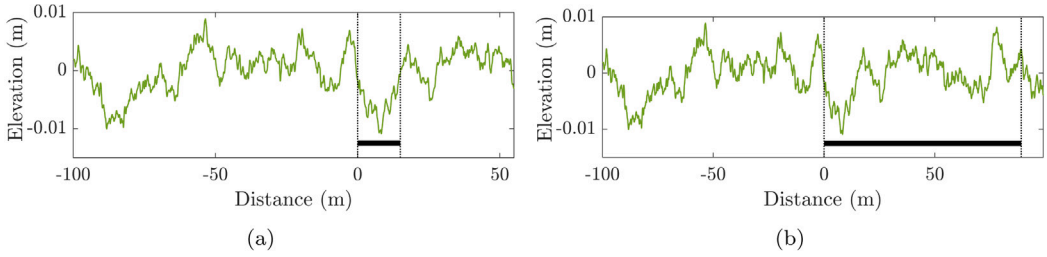

Fig. 6. Road profile of class A and location of bridges (black lines); (a) for study with 15 m simply supported bridge; (b) for study with multi-span continuous bridge.

responses (accelerations, velocities and displacements) of all DOFs of vehicle and bridge. The VBI analysis is carried out by integrating the equations of motion using Newmark-β scheme and implemented in MATLAB [42]. For more details about the coupling procedure and the solution method, the reader is referred to [43].

4. Validation of proposed method

This section applies the proposed damage detection method to 2 separate case studies. Each case study is investigated for a range of damage cases, information scenarios and simulation modes. Fig. 7 provides a schematic overview of all the possibilities considered in this study. The case study A is based on a relatively short simply supported reinforced concrete bridge. It is used to investigate the performance of the proposed method for different damage cases and information scenarios for simulation mode 1 only. At the same time, this case study is used as an example to explain in detail several aspects of the proposed method. In case study B, the method is applied to a multi-span continuous bridge to evaluate the influence of environmental (temperature) and operational effects (additional traffic) by considering different simulation modes (Fig. 7). For both case studies, the crossing vehicles are modelled as fleet of similar vehicles. To model the fleet of the vehicle the variation in vehicles properties is applied to account for normal fluctuations in payload and the inherent uncertainties of the mechanical properties of each vehicle.

4.1. Case study A: Simply supported bridge

4.1.1. Data generation

In this case study, 5-axle trucks travelling over a class A road profile traversing a simply supported bridge, as shown in Fig. 5, are simulated with the vehicle-bridge interaction model presented in Section 3. The FEM of the bridge consists of 30 elements for a total span length L of 15 m. The corresponding section and material properties are: second moment of area $I = 0.5273$ m^4, mass per unit length $\rho = 28\,125$ kg/m, modulus of elasticity $E = 3.5{\times}10^{10}$ N/m^2, and 2% damping. To simulate bridge damage, a localised stiffness reduction in a beam element is considered. In particular, 5 different locations along the beam length are studied with 3 different damage magnitude levels $(15\%, 30\%, 45\%)$ for each location. Therefore, the list of all different damage cases is:

- Healthy case
- Section $L/4$ and stiffness reductions of: 15%, 30%, 45%
- Section $3L/8$ and stiffness reductions of: 15%, 30%, 45%
- Section $L/2$ and stiffness reductions of: 15%, 30%, 45%
- Section $5L/8$ and stiffness reductions of: 15%, 30%, 45%
- Section $3L/4$ and stiffness reductions of: 15%, 30%, 45%

The dataset is generated considering the variation in vehicle properties in such a way that it mimics a fleet of similar vehicles crossing the bridge. The vehicle properties are randomly sampled considering the statistical variability presented in Table A.1. For each of the 16 damage cases, 1000 vehicle passages are simulated, which results a in total 16 000 crossing events. Each event in the dataset contains the information from both, vehicle and bridge. For the 5-axle truck, acceleration measurements from all five axles $\ddot{u}_{a_i}$ is available with a sampling rate of 1000 Hz, as well as, the vehicle speed v, the static axle loads and the ambient temperature. As for the bridge, acceleration readings $\ddot{a}_{br_i}$ are available from 3 assumed sensors installed on the bridge, as indicated in Fig. 8.

The length of the acceleration signals is not the same for all events because the vehicle speed v was randomly sampled for each vehicle

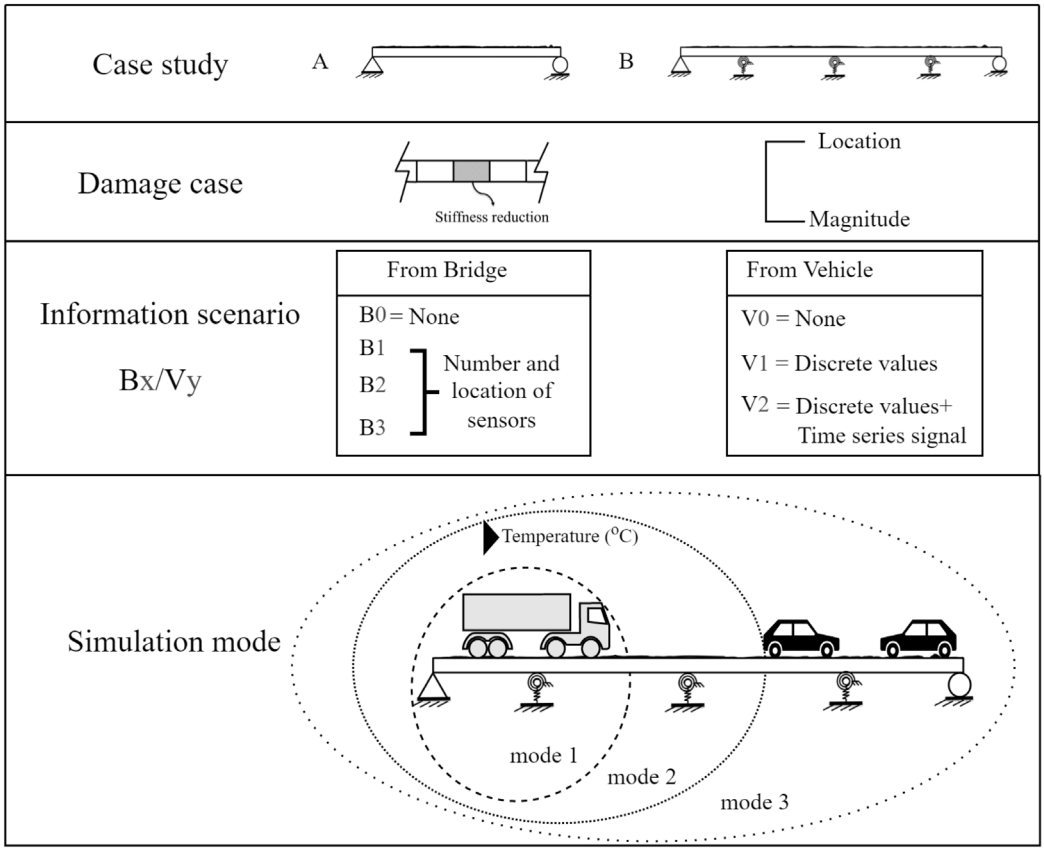

Fig. 7. Overview the possibilities considered in the numerical studies to evaluate the proposed damage detection method.

passage. For the PDNN input, equal length accelerations signals are obtained by zero padding the signals. The length of the required signals depends on the minimum vehicle speed v in the dataset. For this study, the input to the time series module is fixed to $T = 3072$. Therefore, the input size for the time series module of dataset X is $(N, 3072, K)$, for N number of events and K number of variables (number of sensors). On the other hand, the size of the input dataset for the discrete feature module is (N, M), where M is number of input features and M is equal to 3. The dataset has a total 16 output labels, namely the healthy case and 15 different damage scenarios.

4.1.2. Pre-processing

It is well known that the road profile has significant impact on vehicle vibrations. Any measured acceleration within a vehicle is dominated by the excitation produced by the road profile. These road induced vibrations generally mask the component directly related to the bridge response. In previous studies, researchers have applied different techniques to remove the effect of the road profile in vehicle accelerations signals. For instance, in [44], the authors compute the residual response of two connected vehicles, which poses the practical limitation of requiring 2 identical vehicles. Then [45] applied a narrow band pass filter to remove the dynamic effect of the road profile. However, this approach requires to have prior knowledge of the bridge's fundamental frequency. It is safe to say that there is a need for a reliable method that can be used to automatically extract the bridge dynamic response from sensors in passing vehicles.

To address this challenge, in the present study the authors employed the Maximal Overlap Discrete Wavelet Packet Transforms (MODWPT) proposed in [46]. A filter bank based on MODWPT is used here to suppress the road profile component from the vehicle's vertical acceleration signals. MODWPT decomposes the signal $x(t)$ into wavelet components of narrow band frequencies using a wavelet filter [46]. The main advantage of MODWPT over the traditional Discrete Wavelet Transform (DWT) is that it can decompose the signal in both low-frequency and high-frequency signals at each level, whereas DWT can only decompose the signal in low frequency signals [47]. For a given signal $x(t)$, MODWPT produces 2^n equivalent wavelet components W_j, where each has a passband range of $F_s/2^{n+1}$, for a sampling frequency F_s and level number n. Then, the sum of all wavelet components is equal to the approximation of the original signal, as shown in Eq. (11). Similarly, the MODWPT partition of the energy at each wavelet component and the sum of the energy over all the wavelet components is equals the total energy of the input signal [48].

$$x(t) = \sum_{j=1}^{n} W_j(t) \tag{11}$$

In the case of a single vehicle passage, when the truck enters the bridge, the response of the first axle $\ddot{u}_{a_1}$ measures the transient response of the bridge as well as the excitation from the road profile. Then, subsequent axles also cross the same locations on the bridge exposed to the same road profile. Therefore, the dynamic response of all axles should contain the same (or similar) contributions from the road profile. Thus, if the component containing the frequency content of the road profile can be identified in the measured dynamic response, then the contribution of the road profile can be eliminated.

To remove the effect of the road profile from the responses of a vehicle travelling with speed v, the MODWPT with $n = 8$ levels is applied to the axle accelerations $\ddot{u}_{a_i}$. Fig. 9(a) shows the energy level of the first 25 wavelet components (out of 256) for axles 1 and 2. The wavelet components 2 and 3 for axle 1 show significant high energy in comparison to the other components. The additional energy in axle 1 at those particular components can be attributed to the transient response of the bridge. Therefore, it is possible to argue that the sum of certain wavelet components (2 and 3 in this case) from all axle signals $\ddot{u}_{a_i}$ contains predominantly the dynamic response of the bridge.

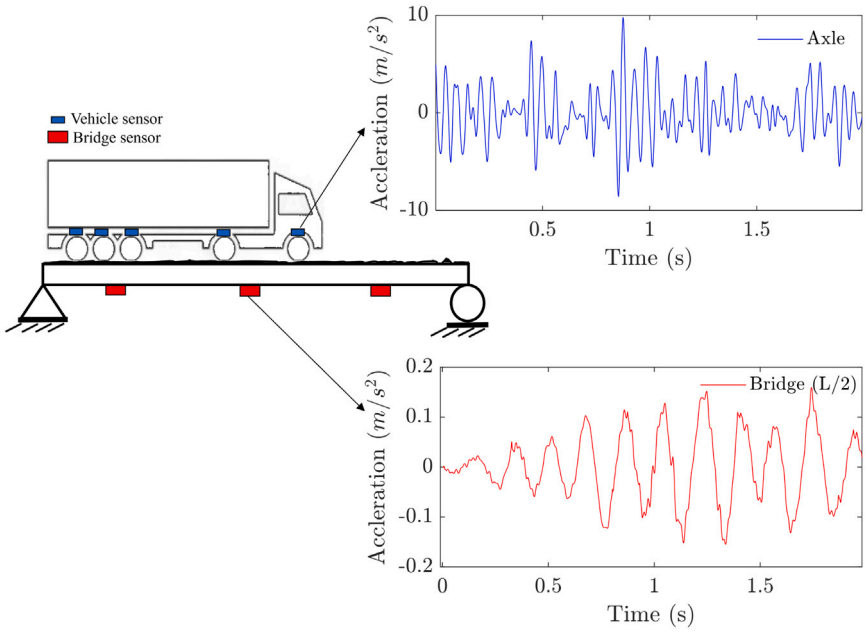

Fig. 8. Samples of signals for case study A.

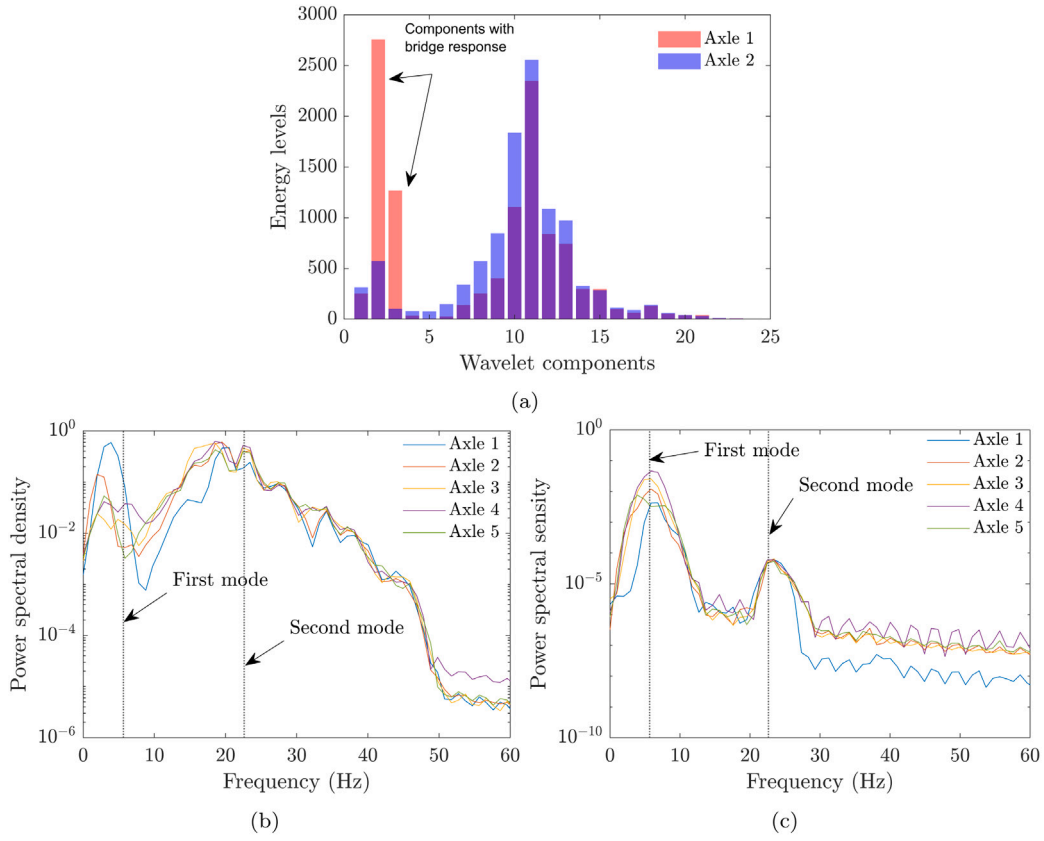

Fig. 9. Pre-processing example; (a) Energy of the wavelet components for axles 1 and 2; (b) Power spectral density of axle responses before applying MODWPT; (c) Power spectral density of axle responses after applying MODWPT.

Fig. 9(b) and (c) show the Power Spectral Density (PSD) of the 5 axle acceleration signals before and after applying MODWPT. The PSD of the raw signals (Fig. 9(b)) shows that the peaks for the first two bridge modes are not distinguishable. However, when the PSD is computed for the sum of the 2nd and 3rd wavelet components, the peaks of first two modes of the bridge are clearly distinguishable (Fig. 9(c)). The advantage of applying MODWPT is clear because it isolates, to a large extent, the contribution of the bridge response in the vehicle acceleration signals. Therefore, the use of filtered vehicle responses via MODWPT is advantageous for structural condition assessment using

drive-by measurements. In this study all vehicle acceleration signals are pre-processed following the procedure discussed in this section.

4.1.3. Evaluation method

In order to demonstrate the performance of the proposed damage detection method, this study considers a range of different information scenarios. Each scenario is defined in terms of the available information for each vehicle crossing event. In some scenarios, the bridge might be instrumented with one or more accelerometers at different sections. In other scenarios, the vehicle might provide no information, discrete values about the event (speed, static axle loads, and temperature), or continuous axle acceleration signals. Thus, several possible scenario exist, which are defined by the amount of information available from both, the vehicle and the bridge. To clearly characterise a given scenario, the following notation has been used:

- B0: No measurement available of the bridge
- B1: Bridge acceleration measurement at section $L/2$
- B2: Bridge acceleration measurement at sections $L/4$ and $3L/4$
- B3: Bridge acceleration measurement at sections $L/4$, $L/2$, and $3L/4$
- V0: No information or measurement available from the vehicle
- V1: Vehicle speed, static axle loads and ambient temperature
- V2: As V1 plus measured axle accelerations

For example, the scenario B1/V2 corresponds to the situation where mid-span bridge accelerations are measured (B1), and the vertical accelerations of all axles of the 5-axle truck are also recorded (V2). Therefore, there exist 10 possible valid scenarios to consider for structural assessment, (since scenarios B0/V0 and B0/V1 do not provide any information about the structure).

The proposed method is applied to these 10 different scenarios, together with a comparative study of the method's performance. Separate PDNN models are created for every information scenario. Fig. 10 shows the flow diagram for training and validation of the PDNN models. More in particular, the datasets are divided into 70–30 splits, for training and validation respectively. For training of the PDNN, a batch size of 128 events is considered, while learning and decay rates are set to $1 \cdot 10^{-4}$ and $1 \cdot 10^{-6}$ respectively, and adaptive moment estimation (Adam) is used as an optimiser. All models are trained using Intel Core i9–10 900 K CPUs with 64 GB RAM and NVIDIA GTX 2080Ti graphic card. Once the model is trained, the single input dataset is evaluated by Monte Carlo based weight sampling from the trained model. The mean value of each prediction by Monte Carlo simulation is computed using Eq. (5). The outcome of the model is the label with the maximum mean probability, and computed using equation Eq. (6).

4.1.4. Results

For the case study A (simply supported beam), the 10 different information scenarios discussed in previous section are studied separately. For each scenario a separate model is trained. The performance of the proposed method for each scenario is evaluated on the basis of overall accuracy of the trained model. The overall accuracy for damage assessment for different combinations of bridge/vehicle information sources is shown in Table 1. It shows that the accuracy of the trained model for scenario B0/V2 (where only vehicle information is available) is equal to 84.2%, which is significantly less compared to the other scenarios. On the other hand, the accuracy of proposed method raises to 91.0% when only using the measurement from a single sensor on the bridge (B1/V0). Then again, the performance of the trained model improves by 4.5 percentage point when including also vehicle axle responses (B1/V2). In addition, the results show that there is no significant performance improvement, in terms of accuracy for damage assessment, when discrete valued vehicle information (V1) is combined with bridge sensors. This can be attributed to the fact that the bridge signals indirectly contain the information (speed and axle loads) of the passing vehicle. Furthermore, accuracy improvements are only marginal in scenarios with multiple bridge signals (B2 and B3) combined with full vehicle information availability (V2). Therefore, the results indicate that a PDNN model can differentiate multiple damage cases with sufficient accuracy solely by extracting damage sensitive features from the bridge signals.

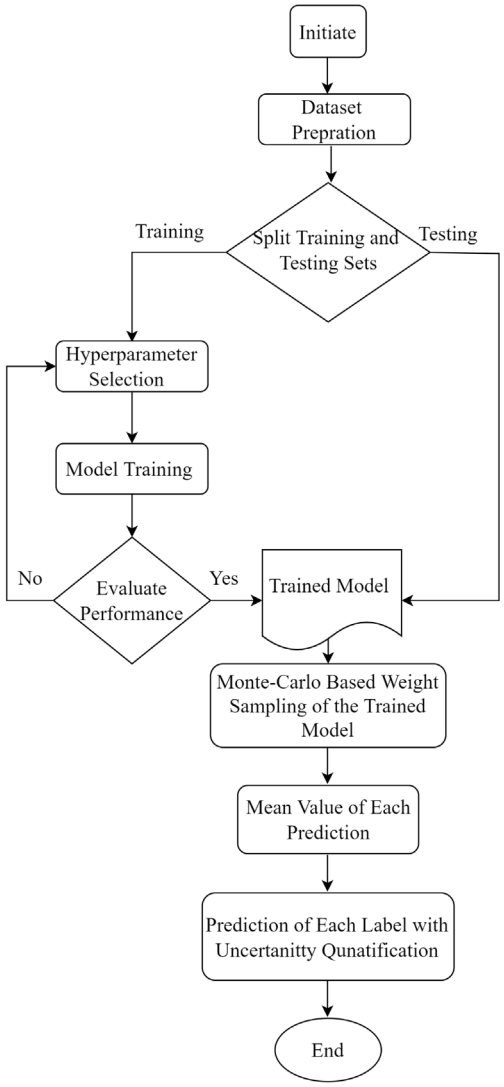

Fig. 10. Flow diagram of probabilistic deep learning model (PDNN).

Table 1
Performance comparison for case study A.

Scenario	V0	V1	V2
B0	NA	NA	84.2%
B1	91.0%	91.2%	95.7%
B2	98.7%	98.9%	99.1%
B3	99.6%	99.2%	99.5%

The performance comparison of the trained models on the validation data provides an indication of the potential use of different information scenarios for damage assessment. But in addition, the use of the PDNN architecture allows us to quantify the uncertainty in the predictions. This is best illustrated with an example. Consider the analysis of a single randomly chosen event crossing a bridge with a 15% damage at section $L/2$. Fig. 11 shows the outputs obtained for different information scenarios in terms of the mean probability of detection of the trained models for different damage labels, computed

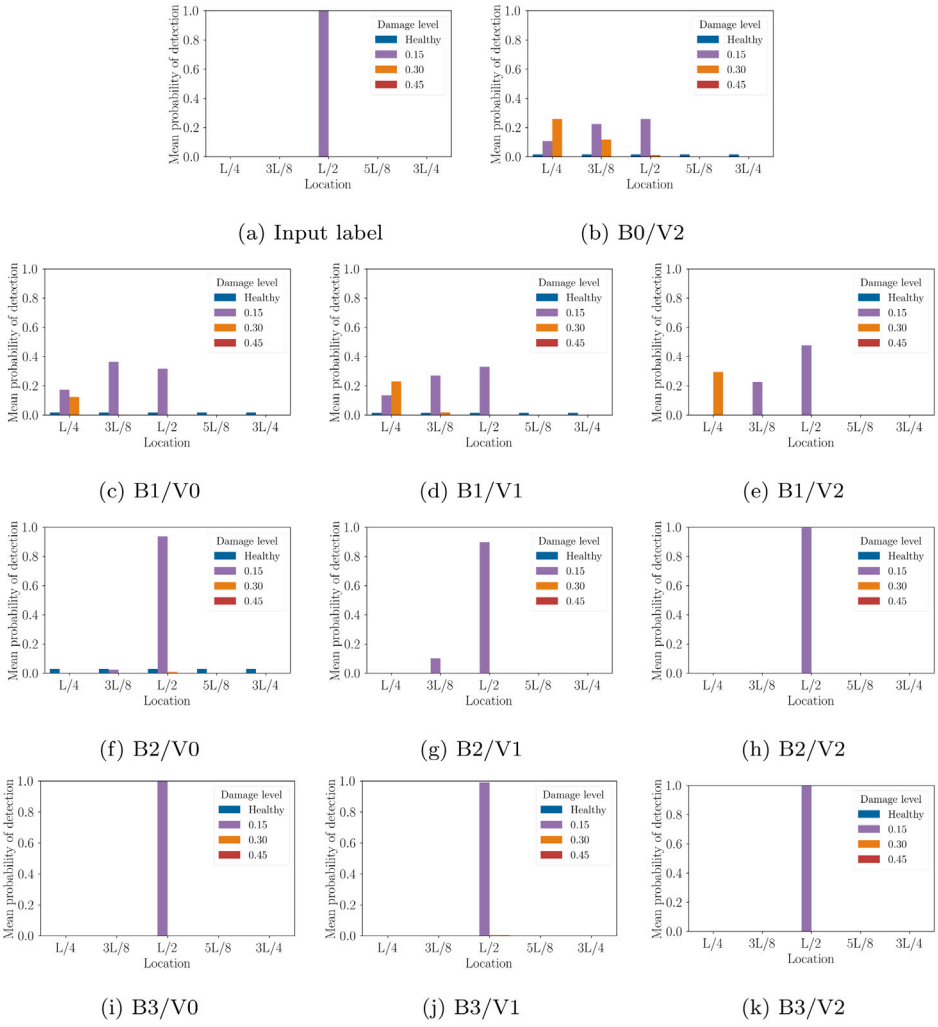

Fig. 11. Damage localisation and quantification, for a single vehicle crossing event in case study A with a 15% damage at L/2 section, for different information scenarios.

using Eq. (6). From the results it can be observed that some scenarios show large uncertainties in damage detection. This is evident, especially in Fig. 11(b), where only vehicle signals are available (B0/V2). The analysis assigns similar mean probabilities to a series of damage cases. There is no clear predominant label. Similarly, when only signals from a single bridge sensor are considered (as in scenarios B1/V0 and B1/V1) the models have difficulties differentiating the exact location and magnitude of the damage, as shown in Fig. 11(c) and (d). However, when the measurement information from the bridge is combined with vehicle sensors (B1/V2), the uncertainty in the decision decreases. Then, the correct label is more prominent (Fig. 11(e)), which indicates that the model in such scenario would be able to locate and quantify the damage. The remaining information scenarios show high and very high certainties providing the correct damage case label.

It is important to stress that the final output decision is solely based on the maximum of the mean probability of detection. Therefore, based on the results in Fig. 11, all the models are able to detect the correct label. From these results, it can be concluded that the PDNN has some difficulty in differentiating damage location and magnitude when only vehicle information is considered. However, by combining sources of information, the damage assessment reliability increases drastically.

4.1.5. Effect of measurement noise

Measurement noise is arguably the most important factor that can affect the performance of the proposed damage assessment procedure. In order to study the effect of noise, white Gaussian noise is added to the acceleration signals by using Eq. (12).

$$\ddot{u}_{polluted} = \ddot{u} + \sigma\, \mathcal{N}(0,\, 1) \tag{12}$$

where $\ddot{u}_{polluted}$ is the noise polluted signal, $\ddot{u}$ is the clean signal, and $\mathcal{N}(0,\, 1)$ is a noise vector with zero mean and unit standard deviation. The standard deviation of the noise component σ is computed using the definition of Signal to Noise Ratio (SNR) as follows:

$$SNR = \frac{P_{\ddot{u}}}{\sigma^2} \tag{13}$$

where $P_{\ddot{u}}$ is the power of the noise-free signal. By using predefined SNR values, the corresponding standard deviation σ of the noise signal can be computed. Often, SNR is given in decibels (dB) and so Eq. (13) can be rewritten as follows:

$$SNR_{dB} = 10\, log_{10}\left(\frac{P_{\ddot{u}}}{\sigma^2}\right) \tag{14}$$

To evaluate the performance of the proposed damage assessment method in the presence of measurement noise, a single random vehicle crossing is studied in detail. The randomly chosen event corresponds to a B0/V2 scenario, i.e., only vehicle information and signals are available. Four different levels of signal to noise ratios (20 dB, 15 dB, 10 dB, and 5 dB) are added to the axle acceleration signals using Eq. (12).

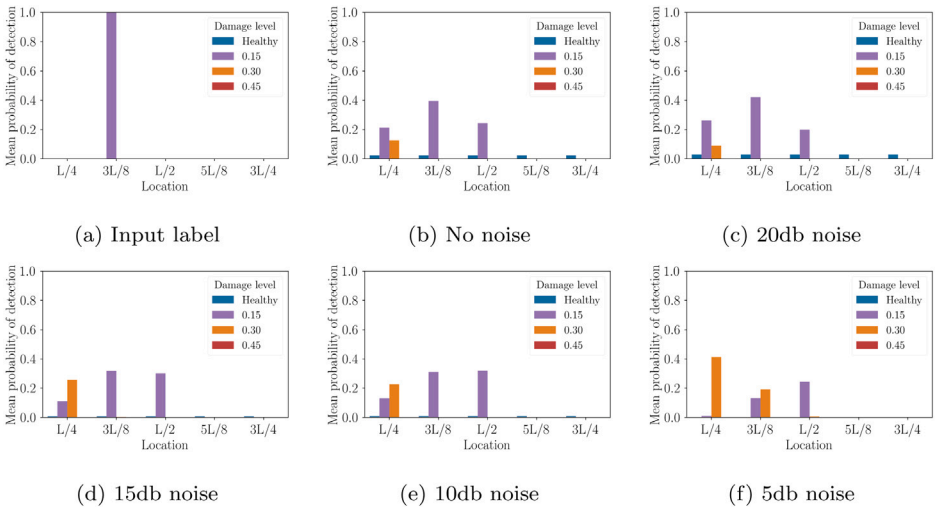

Fig. 12. Effect of measurement noise on damage localisation and quantification for a single crossing event in a B0/V2 scenario.

Fig. 12 shows the results of the sensitivity analysis of measurement noise for damage assessment. The input label shows that the considered event has damage at section $3L/8$ with a 15% stiffness reduction. Fig. 12(b), (c), and (d), show the output prediction of the PDNN models with no noise, 20 dB and 15 dB respectively. For these cases, the trained models are able to localise and quantify the damage with similar levels of uncertainty in the output. However, for larger levels of noise, the performance reduces. For the case of 10 dB SNR (Fig. 12(e)), the output of the model is not able to identify the correct label of damage and instead shows almost equal probabilities for three different damage cases. In the case of very high noise (5 dB SNR), as reported in Fig. 12(f), the PDNN mode failed to quantify and localise the damage case completely. The results from this analysis highlight that the proposed PDNN-based procedure is capable of compensating for normal operational levels of noise, but ceases to work for large noise levels.

4.2. Case study B: Multi-span continuous bridge

4.2.1. Data generation

This section evaluates the proposed damage detection method applied to the case of an existing multi-span continuous bridge. The Voigt Drive I-5 bridge, shown in Fig. 13, is a reinforced concrete box girder bridge with 4 spans and a total length of 89 m [49]. The bridge is simulated as an updated FEM with 0.5 m long beam elements. The section properties have been computed using the actual material properties and cross section dimensions shown in Fig. 13(b). The column supports of the continuous beam model are represented using vertical and rotational springs, of stiffness K_v and K_r respectively. The values for these stiffness have been tuned to match the first three measured frequencies of the original bridge [49]. The final list of the updated bridge properties is presented in Table 2. In addition, and similar to case study A, a road profile of class A is considered with a 100 m approach distance shown in Fig. 6(b).

In line with case study A, damage is modelled as local stiffness reductions also in case study B. But because it is a different bridge, different damage cases have been defined to evaluate the performance the PDNN-based procedure. The Damage Cases (DC) considered in case study B are:

- DC0: Healthy case
- DC1-DC2: Damage at mid-span of span 2 with stiffness reductions of: 30%, 45%
- DC3-DC4: Damage at mid-span of span 3 with stiffness reductions of: 30%, 45%

Table 2
Multi-span bridge model properties.

Description	Symbol	Value
Total span length (m)	L	89
Young's modulus (N/m^2)	E	$3.5 \cdot 10^{10}$
Second moment of area (m^4)	I	1.3427
Cross-section area (m^2)	A	5.6180
Mass per unit length (kg/m)	ρ	2500
Rotational stiffness (N m/rad)	$K_{r,(1,2,3)}$	$4.5 \cdot 10^9$
Vertical stiffness (N/m)	$K_{v,(1,2,3)}$	$3.5 \cdot 10^{10}$
First three modal frequencies (Hz)	$f_{(1,2,3)}$	[4.91, 6.54, 13.45]

- DC5-DC6: Stiffness reduction of 30% at supports 1 and 2

The dataset for this case study is generated by solving the vehicle-bridge interaction model presented in Section 3. To examine the sensitivity of the PDNN method in realistic situations, three simulation modes are examined. Mode 1 considers events with individual 5-axle trucks crossing the multi-span bridge. In addition, simulation mode 2 includes the environmental effect of daily and seasonal temperature variations. Finally, in mode 3, the simulation includes random traffic on the bridge, in addition to the individual 5-axle trucks and temperature oscillations. The dataset for all these three simulation modes is generated considering the statistical variability of the 5-axle truck parameters, by means of Monte Carlo analysis. For Modes 2 and 3, the environmental effect is included by modelling the temperature dependency of concrete's elastic modulus, which is discussed in greater detail in the following subsection. The additional random traffic in mode 3, is modelled including 2-axle vehicles with randomly sampled entry times, speeds, travelling directions and mechanical properties. Additional information about the 2-axle vehicle model and its corresponding parameter values are included in Appendix.

For each simulation mode, separate datasets are generated for different information scenarios. As in the analysis for case study A, these scenarios are defined in terms of the available information from the bridge and the passing vehicles. For the latter, the same definitions for V0, V1 and V2 are used as in Section 4.1.3. However, because the modelled bridge is different now, the information scenarios regarding the available bridge information is different. Case study B defines the possible bridge instrumentation with four accelerometers $\ddot{a}_{b_i}$ as shown in Fig. 13(a). The corresponding bridge information scenarios considered now are listed below.

- B0: No measurement available of the bridge

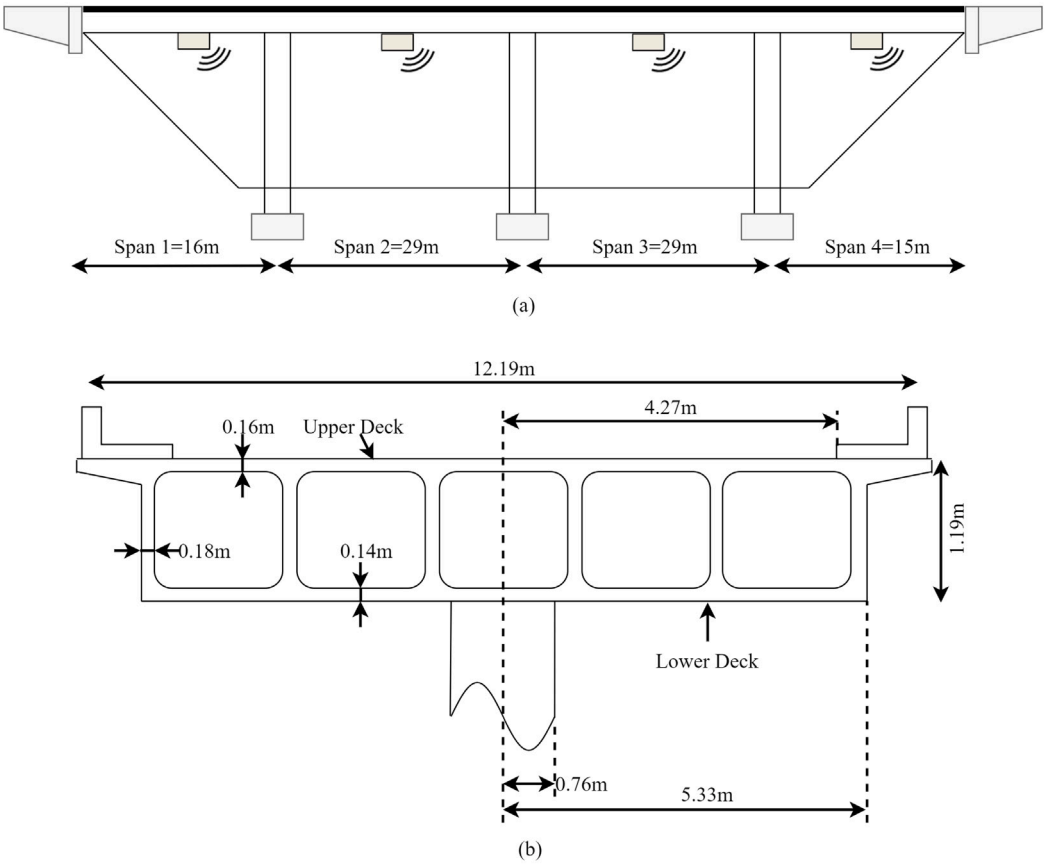

Fig. 13. Voigt Drive/I-5 Bridge; (a) Multi-span bridge model; (b) Cross-section.

- B1: Bridge acceleration measurements at mid-span of spans 1 and 4
- B2: Bridge acceleration measurements at mid-span of spans 2 and 3
- B3: Bridge acceleration measurements at mid-span of all spans

Therefore, this section considers 7 different bridge conditions for each of the 10 valid information scenarios, for each of the 3 simulation modes. Each of the 21 datasets consist of batches of 1000 vehicle crossing events with randomly sampled configurations and properties. These datasets are pre-processed as in Section 4.1.2 to remove the contribution of the road profile from the vehicle signals. The PDNN models are trained using the same hyperparameters, and the datasets are divided in 70–30 splits for training and validation respectively.

4.2.2. Modelling the effect of temperature

In long-term bridge monitoring, variation in temperature plays an important role because it directly influences the material properties of the bridge. As a result the structure experiences changes of its modal properties, that ultimately lead to different dynamic behaviour for the same load. Temperature dependent material properties have been included in the VBI model in order to evaluate the performance of the proposed PDNN model in the presence of oscillating temperatures. This subsection explains how the effect of temperature variation has been modelled.

Concrete's elastic modulus depends on the material's temperature, and this relationship can be linearised for typical ambient temperature ranges [50,51]. It is also known that this linear relationship is different for temperatures below the freezing point [52]. Such bi-linear relationships have been reported, for instance, at the Dowling Hall Foot bridge [53]. Nevertheless, modelling the relationship between temperature and elastic modulus is not a straightforward task and depends on structure's type, location, and environmental conditions. To solve this, empirical models from bridge measurements can be leveraged to establish the relationship between temperature and changes in bridge properties. One such model was developed in [53], where the authors proposed the bi-linear equation for bridge elastic modulus as given in Eq. (15).

$$E_T = E_0 \left[Q + S\,T + R\left(1 - erf\left(\frac{T-\kappa}{\tau}\right)\right)\right] \tag{15}$$

In Eq. (15), E_T is the temperature dependent elastic modulus and E_0 is its value for a reference temperature. The linear relationship is defined in terms of the parameters Q and S, while the term $R\left(1 - erf\left(\frac{T-\kappa}{\tau}\right)\right)$ modifies the relationship for temperatures below zero. In Eq. (15), T is the temperature in degrees Celsius, while κ and τ are the parameters that govern the transition around the freezing point. More details about the temperature dependency of concrete and the model parameters can be found in [54].

In the present study, the influence of temperature has been simulated considering a 2 year temperature record obtained from a weather station in Trondheim (Norway), shown in Fig. 14. For simulation modes 2 and 3, temperature for each crossing event was randomly sampled from these records. Then, the elastic modulus of the concrete was adjusted accordingly using Eq. (15). The parameters in this relationship are also sampled randomly to account for possible uncertainties, as suggested in [54], based on the mean and standard deviation values given in Table 3.

4.2.3. Results

This section reports the results of the proposed damage detection method applied to the case of the multi-span bridge considering the damage cases discussed in Section 4.2.1. The results are presented in a similar format as for case study A. The performance test results for

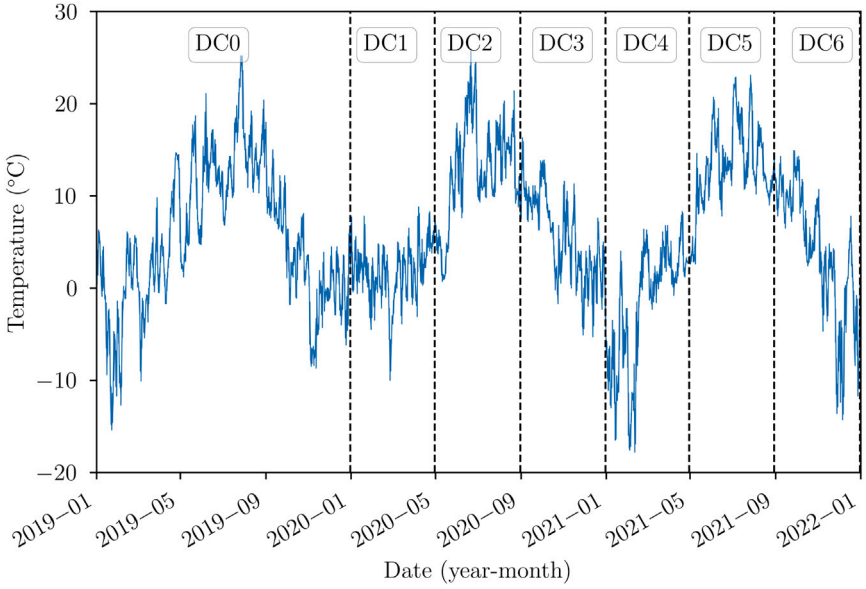

Fig. 14. Daily average temperature record of Trondheim (Norway), and corresponding damage case considered on the bridge.

Table 3
Mean and standard deviation of parameters modelling the effect of temperature on concrete's elastic modulus.

	Q	S	κ	τ	R
μ	1.0129	−0.0048	0.1977	3.1466	0.1977
σ	0.003	0.0001	0.0027	0.0861	0.0027

Table 4
Performance comparison for multi-span bridge case and simulation mode 1.

Scenario	V0	V1	V2
B0	NA	NA	96.1%
B1	97.2%	97.4%	97.4%
B2	98.1%	98.3%	99.0%
B3	98.2%	98.7%	99.2%

Table 5
Performance comparison for multi-span bridge case and simulation mode 2.

Scenario	V0	V1	V2
B0	NA	NA	74.6%
B1	89.2%	90.4%	81.4%
B2	93.9%	94.3%	92.8%
B3	94.2%	94.7%	95.6%

each information scenario, are presented in a table format, indicating the overall accuracy of the trained models. However, in case study B, the analysis is repeated for 3 simulation modes, namely mode 1 (single 5-axle events), mode 2 (with additional temperature variations) and mode 3 (with additional random 2-axle traffic), as discussed in Section 4.2.1.

The results for mode 1 are reported in Table 4. It shows that the PDNN-based approach exhibits comparatively high accuracy in damage assessment for all scenarios. This is even the case for the B0/V2 scenario, where only vehicle sensor information is used. The overall accuracy in this scenario is good (96.1%), and much better that the corresponding result in case study A (see Table 1), which was 84.2%. This improvement is attributed to the duration of the crossing event. Vehicles traversing a longer bridge, spend more time interacting with the structure, which results in longer signals for the proposed method. In addition, the vehicle to mass ratio decreases drastically, ensuring that there is practically no variation of the bridge's modal properties during the crossing event. It is also worth noting that the damage cases considered in case study B are more distinct, as opposed to those considered in case study A. This makes each label (damage case) more distinctive, which facilitates the classification task. The combination of these reasons allow the PDNN model to generalise more precisely the damage sensitive features, leading to the improved accuracy observed in case study B for simulation mode 1.

Table 5 presents the overall performance results for simulation mode 2. In this mode the temperature variations have been included in the simulation, affecting directly the elastic modulus of the bridge model, as discussed in Section 4.2.2. In the simulated information scenarios the temperature is provided by the passing vehicles, and therefore only available in scenarios with V1 and V2. In this setup, it is possible to study what is the effect of that additional information on the performance of the PDNN-based models. By direct comparison of the results between V0 and V1 scenarios, it can be seen that adding the temperature information as input has little impact on the overall accuracy of the models. In addition, the accuracy improvements are of similar magnitude as those reported for mode 1 (where no temperature variations were considered). However, there is an overall decrease in accuracy compared to mode 1 results. This is because the varying temperature creates fluctuations in bridge modal properties (especially first and second mode), which mask the variations associated to small damage cases. This temperature effect is particularly relevant in scenarios using vehicle information (V2). The pre-processing of the vehicle signals effectively isolates the first and second frequencies of the bridge, as shown in Fig. 9(c). As a result of this pre-processing, the PDNN model is not able to properly classify the less severe damage cases, which contributes to the decrease in overall accuracy for scenario B0/V2 reported in Table 5. Compared to bridge only scenarios, where the signals contain the full spectrum, the proposed model can successfully generalise the feature space and thus classify different damage cases more accurately. Furthermore, the results show that when V2 information is combined with B1 and B2 the accuracy of the model decreases. This decrease in accuracy is attributed to the relative weight given by the model to the actual input signals. In B1/V2 and B2/V2 the inputs to the model are 5 vehicle signals and 2 bridge responses. The model gives more weight to the vehicle signals, which are affected more by the effect of temperature variations, resulting in a decrease in accuracy.

Simulation mode 3 imitates the actual operational conditions found in a real case. The bridge vibrations captured by the passing 5-axle

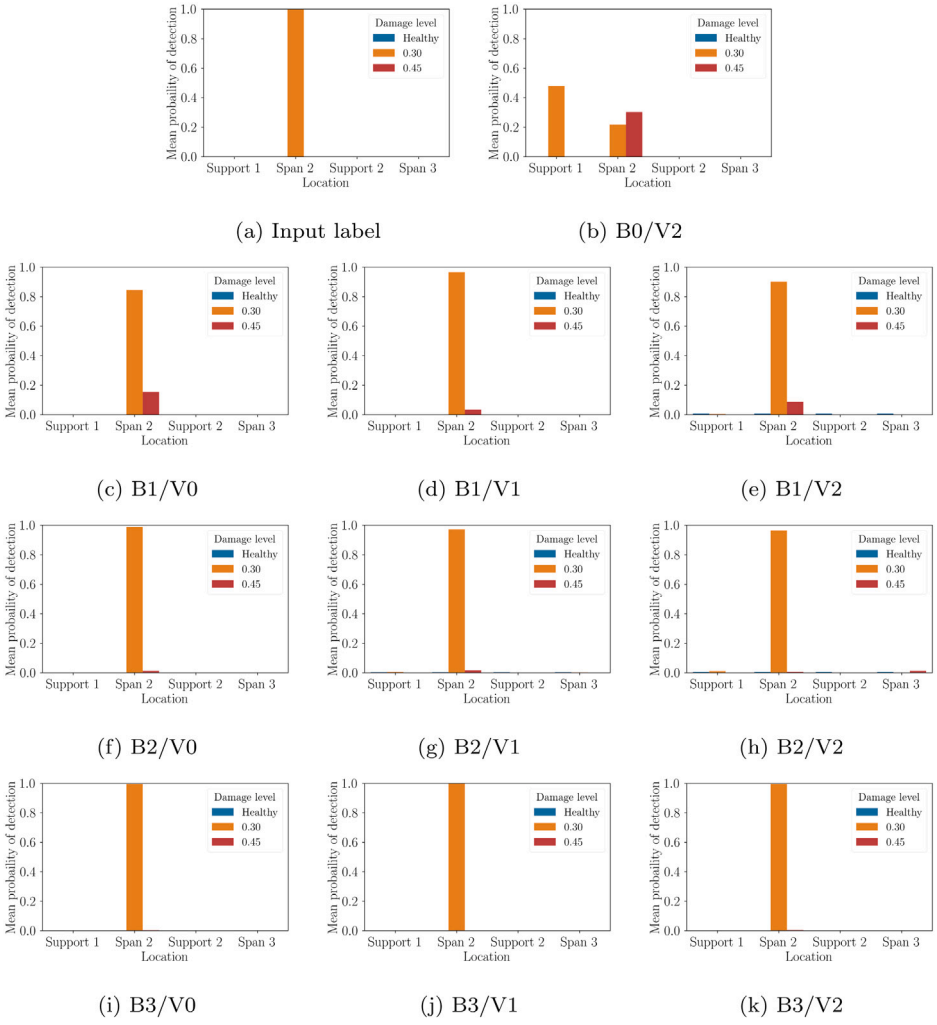

Fig. 15. Effect of measurement information scenario on the accuracy for damage localisation and quantification, for case study B and simulation mode 3.

trucks are affected by the continuous oscillations in ambient temperature and the disturbances induced by additional traffic. The performance results for mode 3 (see Table 6) indicate overall performance reduction but similar trends as those reported for mode 2. Vehicle responses are highly influenced by temperature and by the presence of random traffic compared to bridge response. This is clearly seen in overall decrease of accuracy for all scenarios when V2 information is combined with bridge sensors as discussed in previous section for mode 2.

However, when compared to the other simulation modes, the performances for mode 3 are significantly lower for all scenarios. This is expected because of the additional random traffic, which is unknown to the models. The PDNN models do not get any information about this extra traffic, because these vehicles are not instrumented. The added mass of these additional vehicles affect the bridge dynamic response. The PDNN-based models achieve a suboptimal generalisation of the feature space, and thus have more difficulties classifying the event among the different damage case labels. This is then reflected in overall poorer accuracy, as reported in Table 6.

Taking advantage of the PDNN architecture, it is possible to explore the uncertainty in the model prediction. The analysis of one single crossing event can be presented in terms of mean probability of detection, as explained in Section 2.2. Here, the analysis is repeated for all information scenarios considering one random event under simulation mode 3, and presented in Fig. 15. In particular, in this event the bridge had a damage at the mid-span section of the second span with a severity

Table 6
Performance comparison for multi-span bridge case and simulation mode 3.

Scenario	V0	V1	V2
B0	NA	NA	44.1%
B1	79.2%	82.0%	60.1%
B2	81.1%	82.3%	76.8%
B3	82.4%	84.1%	82.1%

of 30% stiffness reduction. The analysis shows that in scenario B0/V2, when only vehicle measurements are available, the PDNN-based model is not able to correctly identify the damage label. The model distributes the probability among 3 different labels, including the correct one (see Fig. 15(b)). The final outcome of the model is selected as the label with greatest mean probability, which in this case is the wrong answer. However, for the rest of information scenarios, the PDNN models are able to correctly identify the damage with very low uncertainty in the output.

Therefore, from these results it can be concluded that random traffic on the bridge adversely effects the damage detection capability of the proposed PDNN-based method. This negative influence is particularly evident for damage assessment using exclusively the signals from passing vehicles. Therefore, the recommendation for drive-by methods in general is to utilise signals from instrumented vehicles that traverse the target bridge without the presence of additional traffic. Furthermore, the presented results also indicate that to reduce the uncertainties in

damage assessment, it is beneficial to combine the vehicles' responses with the signals from a limited number of sensors mounted on the bridge.

5. Discussion

The results presented here provide the proof of concept for the applicability of vehicle assisted bridge monitoring. The study demonstrates the merits of combining multiple sensory information, including fixed sensor as well as moving sensors (vehicle mounted). The strengths of the proposed PDNN model approach are: (1) scalability, because the proposed method can easily incorporate different types of measurements for damage assessment tasks; (2) robustness, because of the inherit probabilistic nature of proposed method, the effect of noise and different loading conditions do not alter the overall accuracy; (3) implementable, because it does not require heavy pre-processing of the measurements since it can work with raw signals; and (4) enhanced performance of damage detection and localisation in comparison to the similar methods reported in literature [23,45], because the proposed method does not only provide the damage detection results but also quantifies the uncertainty in the output decision.

Furthermore, the novelty of the proposed method can be summarised in three points. First, the proposed PDNN model can combine multiple sensors and extract the damage sensitive features without any pre-processing of the input signals, even when considering realistic operational conditions. The accuracies of damage assessment results for different sensor combinations highlight the ability of the proposed model to distinguish small changes in structural dynamic characteristics. Secondly, compared to other commonly used data driven methods, the proposed PDNN model provides additional insights, since it can quantify the reliability of the model's decision. In previous studies reported in literature, the deep learning models have been trained with fixed weights. This makes their generalisation ability highly susceptible to changing operational and environmental conditions. The proposed PDNN model addresses this issue by replacing fixed weights by probabilistic distributions of weights. This, not only enhances the generalisation ability of the PDNN model, but also quantifies the reliability of the decision making. Lastly, this study can be used as a guideline for future planning of bridge health monitoring systems in practice. The study comprehensively discussed multiple bridge health monitoring scenarios for different levels of damage. Bridge owners can greatly benefit from this study while considering their needs for a monitoring campaign for a particular bridge.

However, there are still some limitations for the implementation of the proposed method. Arguably, the main limitation is related to the requirement of damage labels while training the proposed PDNN model. At present, this can be addressed by combining hybrid approaches and transfer learning techniques, as discussed in [55]. In a hybrid approach, the target bridge labels can be acquired from numerical simulations from Finite element model (FEM) of the bridge and then further combined with real measurements of the bridge for further damage assessment. Nevertheless, this line of work still requires more studies to properly demonstrate the ability for damage assessment in a real life implementation. The other minor limitation is the requirement of synchronised signals from multiple sensors. This can be addressed by adequately utilising existing technologies.

6. Conclusions

This paper has explored the feasibility of vehicle assisted monitoring for damage assessment. The study had two main objectives; (1) to develop a damage assessment method by combining direct and indirect measurement response; (2) to study and quantify the influence of different sensor information combinations. To that end, a probabilistic deep neural network (PDNN) based method was proposed, which is capable of quantifying the uncertainty of its predictions under varying operational and environmental conditions. The effectiveness of the proposed method was evaluated with two case studies, which consisted of 5-axle trucks traversing a simply supported beam and a multi-span continuous bridge. These studies considered several damage cases and investigated the effect of measurement noise, temperature variations, and random traffic. The main findings of this study can be summarised as follows:

- The overall results suggest that vehicle assisted monitoring has the potential to detect small and realistic damage cases under the influence of varying operational and environmental conditions.
- By employing the wavelet transform based filter bank the contribution of the road profile can be removed from vehicle responses which is one of the main hinders in deployment of on-board vehicle sensors for structural damage assessment.
- The combination of sensor information from vehicle and bridge enables a more reliable damage assessment with lower uncertainty in the decision making.
- Random traffic on the bridge adversely affects the ability of the proposed method to detect and localise the damage, when only vehicle sensors are used. Thus, is drive-by or indirect monitoring strategies, it is recommended to use only vehicle responses with no additional traffic present on the bridge.
- Road authorities and bridge owners can use the proposed probabilistic deep neural network based method as a reliable decision making tool for damage assessment.

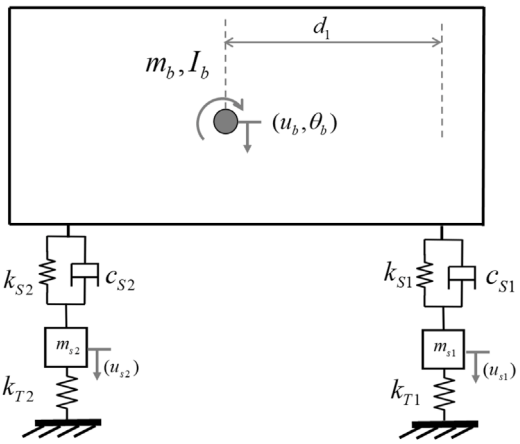

Fig. A.1. 2-axle vehicle model.

CRediT authorship contribution statement

Muhammad Zohaib Sarwar: Conceptualization, Methodology, Software, Investigation, Formal analysis, Writing – original draft. **Daniel Cantero:** Conceptualization, Software, Writing – review & editing, Resources, Supervision.

Declaration of competing interest

The authors declare that they have no known competing financial interests or personal relationships that could have appeared to influence the work reported in this paper.

Data availability

Data will be made available on request.

Table A.1
5-axle truck model parameters.

Parameters	Min.	Max.	Mean	SD
Mass (kg)				
Tractor body m_{b1}	2800	3400	3100	80
Trailer body m_{b2}	15 000	25 000	20 000	1000
Tractor axles m_{u1}, m_{u2}	500	1000	750	30
Trailer axles m_{u3}, m_{u4}, m_{u5}	800	1400	1100	50
Moment of inertia (kg m^2)				
Tractor body I_{b1}	4250	5500	4875	50
Trailer body I_{b2}	112 000	135 000	123 000	2500
Spring stiffness (N/m)				
Tractor suspension k_{S1}, k_{S2}	$4.0 \cdot 10^6$	$8.0 \cdot 10^6$	$6.0 \cdot 10^6$	$0.5 \cdot 10^6$
Trailer suspension k_{S3}, k_{S4}, k_{S5}	$5.0 \cdot 10^6$	$15.0 \cdot 10^6$	$10.0 \cdot 10^6$	$0.5 \cdot 10^6$
Tractor tyre k_{T1}, k_{T2}	$1.3 \cdot 10^6$	$2.3 \cdot 10^6$	$1.8 \cdot 10^6$	$0.2 \cdot 10^6$
Trailer tyre k_{T3}, k_{T4}, k_{T5}	$2.8 \cdot 10^6$	$4.8 \cdot 10^6$	$3.5 \cdot 10^6$	$0.2 \cdot 10^6$
Viscous damping (N s/m)				
Tractor suspension c_{S1}, c_{S2}	$1.0 \cdot 10^4$	$8.0 \cdot 10^4$	$4.0 \cdot 10^4$	$0.5 \cdot 10^4$
Trailer suspension c_{S3}, c_{S4}, c_{S5}	$2.0 \cdot 10^4$	$16.0 \cdot 10^4$	$8.0 \cdot 10^4$	$1.0 \cdot 10^5$
Geometry (m)				
b_1	3.50	6.50	5.00	0.10
a_2	3.00	5.00	4.00	0.02
d_1	−0.50	−1.20	−1.09	−0.01
d_2	3.00	4.00	3.50	0.05
d_3	–	–	1.20	–
d_4	–	–	2.20	–
d_5	–	–	3.20	–
Velocity (km/h)				
Velocity	36	72	54	8

Table A.2
2-axle truck model parameters.

Parameters	Min.	Max.	Mean	SD
Mass (kg)				
Body mass m_{b1}	5000	16 000	10 500	500
Tractor axles m_{u1}, m_{u2}	600	1200	900	100
Moment of inertia (kg m^2)				
Body I_b	45 000	65 000	53 651	2000
Spring stiffness (N/m)				
Suspension k_{S1}, k_{S2}	$4.0 \cdot 10^6$	$8.0 \cdot 10^6$	$6.0 \cdot 10^6$	$0.5 \cdot 10^6$
Tyre K_{T3}, K_{T4}	$1.25 \cdot 10^6$	$2.25 \cdot 10^6$	$1.75 \cdot 10^6$	$0.20 \cdot 10^6$
Viscous damping (N s/m)				
Suspension c_{S1}, c_{S2}	$0.5 \cdot 10^4$	$1.5 \cdot 10^4$	$1.0 \cdot 10^4$	$0.2 \cdot 10^4$
Geometry (m)				
d_1	4	6	–	–
Velocity (km/h)				
Velocity	36	72	54	8

Appendix

Table A.1 provides the numerical values of the parameters for the 5-axle truck model, together with their statistical variability, used for the Monte Carlo simulations. Similarly, Table A.2 provides the model parameter for the 2-axle vehicle model (shown in Fig. A.1), which is used to simulate the additional random traffic in case study B (Section 4.2).

References

[1] O. Avci, O. Abdeljaber, S. Kiranyaz, M. Hussein, M. Gabbouj, D.J. Inman, A review of vibration-based damage detection in civil structures: From traditional methods to Machine Learning and Deep Learning applications, Mech. Syst. Signal Process. 147 (2021) 107077.

[2] L. Quirk, J. Matos, J. Murphy, V. Pakrashi, Visual inspection and bridge management, Struct. Infrastruct. Eng. 14 (3) (2018) 320–332.

[3] Y. An, E. Chatzi, S.-H. Sim, S. Laflamme, B. Blachowski, J. Ou, Recent progress and future trends on damage identification methods for bridge structures, Struct. Control Health Monit. 26 (10) (2019) e2416.

[4] P. Singh, A. Sadhu, Limited sensor-based bridge condition assessment using vehicle-induced nonstationary measurements, in: Structures, Vol. 32, Elsevier, 2021, pp. 1207–1220.

[5] S. Wang, E.J. OBrien, D.P. McCrum, A novel acceleration-based moving force identification algorithm to detect global bridge damage, Appl. Sci. 11 (16) (2021) 7271.

[6] H. Shokravi, H. Shokravi, N. Bakhary, M. Heidarrezaei, S.S. Rahimian Koloor, M. Petr, Vehicle-assisted techniques for health monitoring of bridges, Sensors 20 (12) (2020) 3460.

[7] E. OBrien, C. Carey, J. Keenahan, Bridge damage detection using ambient traffic and moving force identification, Struct. Control Health Monit. 22 (12) (2015) 1396–1407.

[8] C. McGeown, F. Huseynov, D. Hester, P. McGetrick, E.J. Obrien, V. Pakrashi, Using measured rotation on a beam to detect changes in its structural condition, J. Struct. Integr. Maint. 6 (3) (2021) 159–166, http://dx.doi.org/10.1080/24705314.2021.1906092, arXiv:https://doi.org/10.1080/24705314.2021.1906092.

[9] E.J. Obrien, J. Brownjohn, D. Hester, F. Huseynov, M. Casero, Identifying damage on a bridge using rotation-based Bridge Weigh-In-Motion, J. Civ. Struct. Health Monit. 11 (1) (2021) 175–188.

[10] Z. Wang, J.P. Yang, K. Shi, H. Xu, F. Qiu, Y. Yang, Recent advances in researches on vehicle scanning method for bridges, Int. J. Struct. Stab. Dyn. (2022).

[11] R. Corbally, A. Malekjafarian, A data-driven approach for drive-by damage detection in bridges considering the influence of temperature change, Eng. Struct. 253 (2022) 113783.

[12] M.Z. Sarwar, D. Cantero, Deep autoencoder architecture for bridge damage assessment using responses from several vehicles, Eng. Struct. 246 (2021) 113064.

[13] R. Corbally, A. Malekjafarian, Examining changes in bridge frequency due to damage using the contact-point response of a passing vehicle, J. Struct. Integr. Maint. 6 (3) (2021) 148–158.

[14] Y. Yang, Y. Li, K.C. Chang, Constructing the mode shapes of a bridge from a passing vehicle: a theoretical study, Smart Struct. Syst. 13 (5) (2014) 797–819.

[15] A. Sumalee, H.W. Ho, Smarter and more connected: Future intelligent transportation system, Iatss Res. 42 (2) (2018) 67–71.

[16] J. Guerrero-Ibáñez, S. Zeadally, J. Contreras-Castillo, Sensor technologies for intelligent transportation systems, Sensors 18 (4) (2018) 1212.

[17] F. Ni, J. Zhang, M.N. Noori, Deep learning for data anomaly detection and data compression of a long-span suspension bridge, Comput.-Aided Civ. Infrastruct. Eng. 35 (7) (2020) 685–700.

[18] Y. Zhang, Y. Miyamori, S. Mikami, T. Saito, Vibration-based structural state identification by a 1-dimensional convolutional neural network, Comput.-Aided Civ. Infrastruct. Eng. 34 (9) (2019) 822–839.

[19] T. Zhang, D. Shi, Z. Wang, P. Zhang, S. Wang, X. Ding, Vibration-based structural damage detection via phase-based motion estimation using convolutional neural networks, Mech. Syst. Signal Process. 178 (2022) 109320.

[20] M. Tabaszewski, G.M. Szymański, T. Nowakowski, Vibration-based identification of engine valve clearance using a convolutional neural network, Arch. Transp. 61 (1) (2022) 117–131.

[21] B. Zhao, X. Zhang, Z. Zhan, Q. Wu, A robust construction of normalized CNN for online intelligent condition monitoring of rolling bearings considering variable working conditions and sources, Measurement 174 (2021) 108973.

[22] X. Ma, Y. Lin, Z. Nie, H. Ma, Structural damage identification based on unsupervised feature-extraction via Variational Auto-encoder, Measurement 160 (2020) 107811.

[23] J. Won, J.-W. Park, S. Jang, K. Jin, Y. Kim, Automated structural damage identification using data normalization and 1-dimensional convolutional neural network, Appl. Sci. 11 (6) (2021) 2610.

[24] C. Szegedy, W. Zaremba, I. Sutskever, J. Bruna, D. Erhan, I. Goodfellow, R. Fergus, Intriguing properties of neural networks, 2013, arXiv preprint arXiv:1312.6199.

[25] L.V. Jospin, H. Laga, F. Boussaid, W. Buntine, M. Bennamoun, Hands-on Bayesian neural networks—A tutorial for deep learning users, IEEE Comput. Intell. Mag. 17 (2) (2022) 29–48.

[26] E. Goan, C. Fookes, Bayesian neural networks: An introduction and survey, in: Case Studies in Applied Bayesian Data Science, Springer, 2020, pp. 45–87.

[27] N.G. Polson, V. Sokolov, Deep learning: A Bayesian perspective, Bayesian Anal. 12 (4) (2017) 1275–1304.

[28] T. Kim, J. Song, O.-S. Kwon, Probabilistic evaluation of seismic responses using deep learning method, Struct. Saf. 84 (2020) 101913.

[29] C. Andrieu, N. De Freitas, A. Doucet, M.I. Jordan, An introduction to MCMC for machine learning, Mach. Learn. 50 (1) (2003) 5–43.

[30] O. Abdeljaber, O. Avci, S. Kiranyaz, M. Gabbouj, D.J. Inman, Real-time vibration-based structural damage detection using one-dimensional convolutional neural networks, J. Sound Vib. 388 (2017) 154–170.

[31] Z. Wang, W. Yan, T. Oates, Time series classification from scratch with deep neural networks: A strong baseline, in: 2017 International Joint Conference on Neural Networks (IJCNN), IEEE, 2017, pp. 1578–1585.

[32] F. Karim, S. Majumdar, H. Darabi, S. Chen, LSTM fully convolutional networks for time series classification, IEEE Access 6 (2017) 1662–1669.

[33] F. Karim, S. Majumdar, H. Darabi, S. Harford, Multivariate LSTM-FCNs for time series classification, Neural Netw. 116 (2019) 237–245.
[34] TensorFlow Probability. URL https://www.tensorflow.org/probability.
[35] Y. Wen, P. Vicol, J. Ba, D. Tran, R. Grosse, Flipout: Efficient pseudo-independent weight perturbations on mini-batches, in: International Conference on Learning Representations, 2018.
[36] D. Cantero, A. González, Bridge damage detection using weigh-in-motion technology, J. Bridge Eng. 20 (5) (2015) 04014078.
[37] D. Cantero, VEqMon2D—Equations of motion generation tool of 2D vehicles with Matlab, SoftwareX 19 (2022) 101103.
[38] N.K. Harris, E.J. OBrien, A. González, Reduction of bridge dynamic amplification through adjustment of vehicle suspension damping, J. Sound Vib. 302 (3) (2007) 471–485.
[39] A. González, O. Mohammed, Dynamic amplification factor of continuous versus simply supported bridges due to the action of a moving vehicle, Infrastructures 3 (2) (2018) 12.
[40] I.M. Vibration, Road Surface Profiles–Reporting of Measured Data; ISO 8608, International Standards Organisation, Geneve, 2016.
[41] X.-Y. Zhou, M. Treacy, F. Schmidt, E. Brühwiler, F. Toutlemonde, B. Jacob, Effect on bridge load effects of vehicle transverse in-lane position: A case study, J. Bridge Eng. 20 (12) (2015) 04015020.
[42] MATLAB, Version 9.10.0 (r2020a), 2022.
[43] D. Cantero, A. González, E.J. O'Brien, Comparison of bridge dynamic amplification due to articulated 5-axle trucks and large cranes, Balt. J. Road Bridge Eng. 6 (1) (2011) 39–47.
[44] Y. Yang, Y. Li, K. Chang, Using two connected vehicles to measure the frequencies of bridges with rough surface: a theoretical study, Acta Mech. 223 (8) (2012) 1851–1861.
[45] W. Locke, J. Sybrandt, L. Redmond, I. Safro, S. Atamturktur, Using drive-by health monitoring to detect bridge damage considering environmental and operational effects, J. Sound Vib. 468 (2020) 115088.
[46] D.B. Percival, A.T. Walden, Wavelet Methods for Time Series Analysis, Vol. 4, Cambridge University Press, 2000.
[47] A.T. Walden, A.C. Cristan, The phase–corrected undecimated discrete wavelet packet transform and its application to interpreting the timing of events, Proc. R. Soc. Lond. Ser. A Math. Phys. Eng. Sci. 454 (1976) (1998) 2243–2266.
[48] P.-W. Shan, M. Li, Nonlinear time-varying spectral analysis: HHT and MODWPT, Math. Probl. Eng. 2010 (2010).
[49] M. Fraser, A. Elgamal, X. He, J.P. Conte, Sensor network for structural health monitoring of a highway bridge, J. Comput. Civ. Eng. 24 (1) (2010) 11–24.
[50] H. Liu, X. Wang, Y. Jiao, Effect of temperature variation on modal frequency of reinforced concrete slab and beam in cold regions, Shock Vib. 2016 (2016).
[51] Y. Xia, H. Hao, G. Zanardo, A. Deeks, Long term vibration monitoring of an RC slab: temperature and humidity effect, Eng. Struct. 28 (3) (2006) 441–452.
[52] B. Peeters, J. Maeck, G. De Roeck, Vibration-based damage detection in civil engineering: excitation sources and temperature effects, Smart Mater. Struct. 10 (3) (2001) 518.
[53] P. Moser, B. Moaveni, Environmental effects on the identified natural frequencies of the Dowling Hall Footbridge, Mech. Syst. Signal Process. 25 (7) (2011) 2336–2357.
[54] I. Behmanesh, B. Moaveni, Accounting for environmental variability, modeling errors, and parameter estimation uncertainties in structural identification, J. Sound Vib. 374 (2016) 92–110.
[55] B.T. Svendsen, O. Øiseth, G.T. Frøseth, A. Rønnquist, A hybrid structural health monitoring approach for damage detection in steel bridges under simulated environmental conditions using numerical and experimental data, Struct. Health Monit. (2022) 14759217221098998.